Postbuckling Behavior of Laminated Composite Stiffeners and Stiffened Panels Under Cyclic Loading

Y. Frostig*
Technion—Israel Institute of Technology, Haifa, Israel
G. Siton† and A. Segal‡
Israel Aircraft Industries, Ben-Gurion Airport, Israel
and
I. Sheinman§ and T. Weller¶
Technion—Israel Institute of Technology, Haifa, Israel

Results of an experimental, analytical study of the postbuckling of selected graphite-epoxy stiffeners subjected to static and cyclic axial compression loading are presented. Postbuckling behavior and failure characteristics are described. Stiffener sections include I and J shapes, commonly used in stiffened panels, with a 12-ply skin attached. Failure of all specimens, regardless of shape, was associated with cap delaminations and cracks and fiber breakage in the attached skin. Analytical results from a computer program analysis of a nonlinear stiffened panel correlated well with postbuckling test results. The analytical modeling necessary to predict accurately the response of the stiffener is described. The cyclic loading has a favorable effect on the failure loads compared with the statically loaded specimens.

I. Introduction

METALLIC stiffened panels and shells are sometimes designed to buckle below the design-limit load. The degree of postbuckling, which depends on the type of structure, is often limited because of nonstructural considerations, such as aerodynamic requirements, etc. Wing and empennage covers are sometimes allowed to buckle below the limit load. Fuselage panels, on the other hand, are usually designed to sustain stresses of three to four times those corresponding to initial buckling. Collapse of such structures is characterized by a ductile failure, e.g., large deformations. This form of collapse is due to the plastic capability of the material.

Design of more efficient composite structures can be achieved if more data on postbuckling behavior and strength become available. Significant weight savings are projected if composite structures can be utilized in the postbuckling region. Presently, graphite-epoxy structures are limited to nonbuckling load levels because of the lack of experimental data and analytical methodology. In fuselage structures, compression members account for a significant percentage of the total structural weight. The ability to increase the load-carrying capacity of these members by operating them in the postbuckling region offers even greater weight savings than heretofore possible.

Failure of compressed stiffened composite panels is usually controlled by the carrying capacity of their stiffeners. A thorough understanding of the stiffener behavior under static and cyclic compressive loads will lead to better predictions of the panel behavior, especially in the postbuckling region, and of failure characteristics. Failure predictions are usually based on the equivalent section concept, e.g., a typical section consisting of stiffener and skin. The attached skin width equals the typical effective width of the panel (see Ref. 16).

In view of these considerations, an investigation was conducted of the initial, local buckling, postbuckling, and crippling behavior of graphite-epoxy stiffeners. Among the important objectives of the study were the following: 1) to evaluate the feasibility of utilizing the postbuckling strength of the stiffener under static and cyclic compressive loading, and 2) to predict the behavior and failure characteristics of a complex structure, like stiffened panels, based on its constituent behavior.

A large number of publications dealing with the postbuckling of metallic panels under compression and shear loads appear in the literature; see, for example, Refs. 1 and 2. During the past few decades, the classical buckling problem was extended, to some extent, to anisotropic plates; see Refs. 3–11. Published research on stiffened composite panels is limited. Leissa[12] cited a few references, using analytical procedures for predicting postbuckling behavior.

A design procedure for stiffened panels appears in Refs. 13 and 14. Starnes and Rouse[9,10] tested a stiffened panel under a static compressive load. The experimental results related well with the analytical results using the STAGSS-C1 code.[9] The failure pattern reported for all of the tested panels started at the interface of the skin and the stiffener, which caused a separation of the stiffener from the skin. Publications on fatigue effects are rarely found in the open literature; among the few that can be cited are Refs. 15 and 16. Renieri and Garrett[17] dealt with the postbuckling of thin-walled compression members under static compressive loads.

This paper describes the results of a study of thin-walled stiffeners with an attached skin. The experimental part includes static as well as a cyclic compression at load levels in the postbuckling range. The analytical part includes results from an in-house developed code, PBCOMP. The program predicts the postbuckling behavior of stiffened panels as well as thin-walled stiffeners and models the structure as separate plates connected through compatibility and continuity conditions. Results include postbuckling behavior at various parts of the structure as well as overall behavior, with coupling between local buckling and overall behavior. The analytical results were in good agreement with the experimental ones.

Presented as Paper 88-5.6.4 at the 16th Congress of the International Council of the Aeronautical Sciences, Jerusalem, Israel, Aug. 28–Sept. 2, 1988; received Aug. 23, 1989; revision received Aug. 9, 1990; accepted for publication Aug. 29, 1990.

*Senior Lecturer, Faculty of Civil Engineering.
†Research Engineer.
‡Manager, Advanced Technologies and Structures, TASHAN Engineering Center.
§Associate Professor, Faculty of Civil Engineering.
¶Associate Professor, Faculty of Aeronautical Engineering.

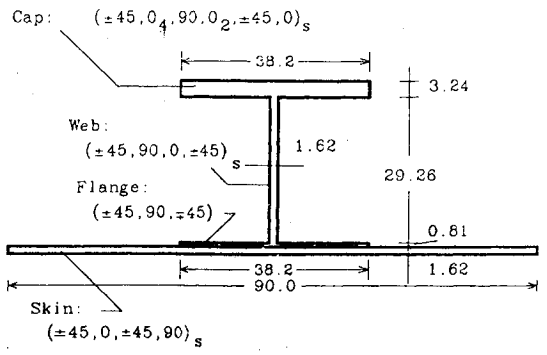

a) I stiffener

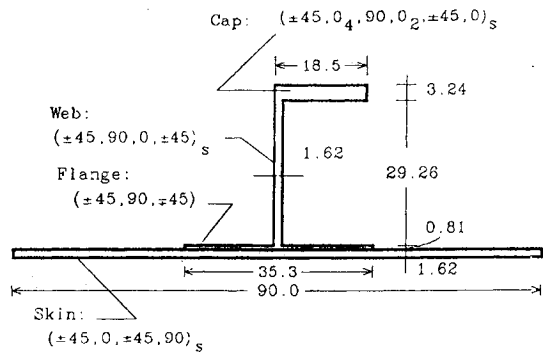

b) J stiffener

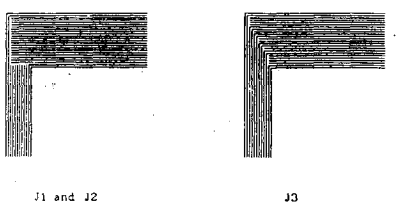

c) Web-cap ply orientation

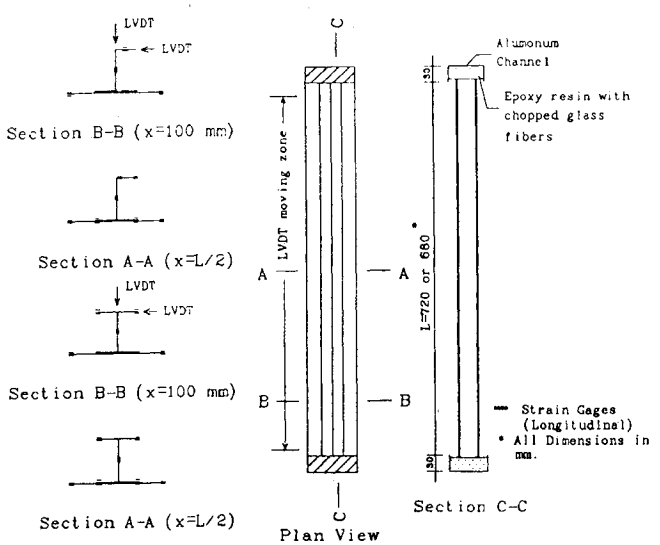

d) Monitoring system setup and end conditions

Fig. 1 Geometry, stacking sequence, web-cap ply orientation, monitoring system setup, and end conditions of typical I- and J-shape stiffeners.

The experimental program is discussed in the next section, followed by the analytical results. The paper concludes with recommendations.

II. Experimental Program

The experimental program included 11 specimens consisting of I- and J-shaped sections (see Figs. 1). Each group consisted of three "long" specimens, 750 mm long, and three "short" ones, 250 mm long. The first group (long) included stiffener section and an attached skin of 90-mm width. The additional skin allowed a modeling of the stiffener behavior within a stiffened panel with the aid of the effective width concept (see Ref. 16). Dimensions and layouts of the two configurations are shown in Figs. 1.

The specimens were designed and manufactured by the Israel Aircraft Industries (IAI) and tested at the Structures Laboratory of the Aeronautical Department at the Technion. The specimens were fabricated of AS4/3502, graphite-epoxy tape material. This material, a 350°F cure type, is commonly used in composite aircraft structures. The manufacturing process consisted of one curing cycle, with the stiffener integrally laid onto the skin and cocured with it.

All specimens were manufactured, in one step, by fabricating a large stiffened panel and cutting it to the proper dimensions. This procedure allowed all specimens to be manufactured under the same conditions. The stiffener skin separation failure mode reported in Refs. 9 and 10 was prevented by overlapping two upper plies of the skin on the lower flange of the stiffeners.

Following curing, the specimens were ultrasonically inspected to establish specimen quality. No defects were detected. The ends of each specimen were embedded in an epoxy resin mixed with chopped glass fibers and encased in a U-shaped aluminum channel. The loaded ends were machined flat and parallel to permit uniform end shortening under compressive loads. The specimens were painted white on both sides to enhance the moire fringe pattern and the fracture visibility of the black graphite fibers.

Strain gauges bonded back to back were placed on the specimens at the following locations: skin edges, intersection point of flange end and attached skin, and the center of web and cap edges. In the J-shaped stiffeners, the web-cap intersection point was monitored too. Out-of-plane and horizontal deflections along the stiffener's caps were monitored with the aid of a moving linear variable deformation transformer (LVDT) apparatus (see Fig. 1d).

The long specimens were used to define local and overall buckling under both static and cyclic compressive loads; the short, to define the crippling load capacity of the stiffeners. The first of each group of long specimens was statically loaded to failure, and the remaining ones were cycled to 250k cycles. The statically loaded specimen results were used to define the initial buckling and the failure load levels were used as reference points. The other specimens were cycled at load levels above the initial buckling reference point. A static residual strength test was conducted upon completion of the cyclic loading program.

The experimental results for each specimen included average and bending (nondimensional curvature) strains and end shortening and displacement vs applied load.

A. I Stiffener

The reference specimen, I1, was monitored by strain gauges at two sections: the first, section B-B, 100 mm from the lower loaded end; the second, section A-A, at the crest of a halfwave. Uniformity and eccentricity of the applied load were monitored by the strain gauges located at section B-B (see Fig. 1c). The buckled-mode shapes were observed with the aid of the moire shadow-fringe technique.

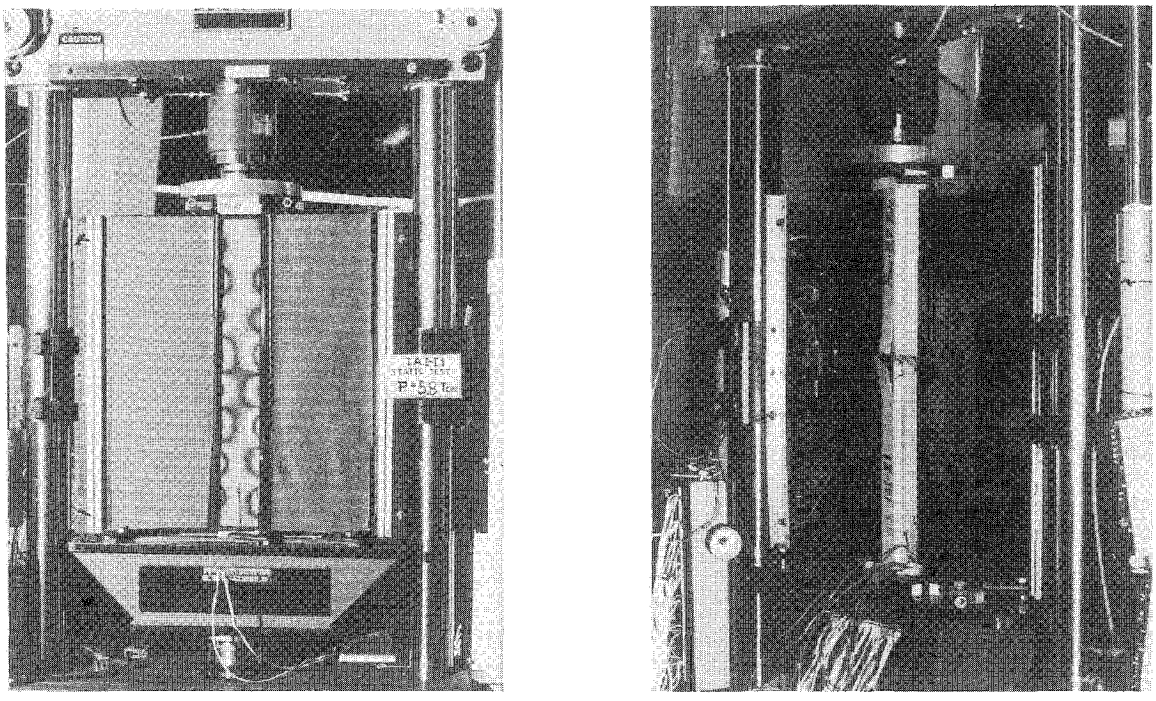

Fig. 2 Specimen I1: a) buckling-mode shapes; b) failure pattern.

The stiffener was statically loaded up to failure to define initial buckling and failure load levels. No initial curvature was observed. Formation of buckling halfwaves, at midspan, started at 4400 kg and was fully formed at 6000 kg (see Fig. 2a). Failure occurred at 8700 kg, whereas prediction, based on an equivalent section and a length of 720 mm, was 9000 kg (see Fig. 2b). Collapse followed the known trends of column buckling associated with delaminations in the cap and cracks and fiber breakage in the attached skin, concentrated at midspan. No separation at the skin-stiffener interface was detected. Initial instability load based on average strains vs applied loads curves at skin edges yielded 4300 kg (see Table 1 for more details).

The second and third specimens were cycled to 250k cycles at load levels around the initial buckling load level of the reference specimen. The monitoring pattern was changed, and the strain gauges were concentrated at the crest of a buckled halfwave to allow for more information on the behavior.

Results here are discussed only for the I2 specimen because the I3 behavior was nearly identical, except for the failure load. The length of these two specimens was shortened to 680 mm due to a premature damage at the lower end. The specimen was statically loaded and then cycled at various load levels (see Table 1). Completion of the cyclic loading program was followed by a residual strength test. The pattern of the buckling-mode shapes is shown in Fig. 3a. Excessive deformations were observed prior to failure (see Fig. 3b). Collapse occurred at 9400 kg, initiated by cracks in the attached skin and followed by delaminations in the cap. Failure pattern was identical with that of the third specimen, I3, but at a lower load (see Fig. 6a). The measured strains were around 0.8–0.9%. Prediction based on gross section yielded a failure load of 11,000 kg.

Table 1 Summary of long I stiffeners, strains, buckling, and failure loads

Specimen	Cyclic loading range, kg	Total number of cycles	Initial buckling		Failure load, kg
			Load, kg	Strains[b]	
I1	Static	——	4250	2082(7)	8,700
			4350	1976(4)	
I2[a]	5000–6000	230,000	3640	1773(4)	9,400
			3800	1732(7)	
I3[a]	5000–6000	240,000	3870	1670(4)	10,200
			3510	1732(7)	

[a]Specimen was damaged at lower end at the beginning of cyclic program.
[b]Numbers in parentheses are strain gauge locations (see Fig. 4). Strains were measured in microstrains, 10^{-6} mm/mm.

The local and overall behaviors are shown in graphical form in Figs. 4 and 5. Total force vs average strains at the attached skin and flange, locations 1–4, appear in Fig. 4a. The behavior changed the trend at the initial buckling load level. Section shape was preserved as long as load level was below initial buckling level. Above it, because of local instabilities in the attached skin, the section shape was deformed. Loss of stability at locations 4 and 7 was associated with lower average strains and very large bending strains (see Fig. 4b). The skin-flange intersection points retained their axial rigidity; thus, a reduction in the compressive strains at the skin edges was accompanied by an increase in the compressive strains at these points. The curvatures or bending strains at the edges of the skin had opposite signs and different absolute values (see Fig. 4b). The deformation prior to failure at location 4 was smaller than at location 7, as shown in Fig. 4b.

One of the questions the study looked into was that of the coupling effects of the local buckling of various parts of the stiffener in the overall behavior. Web average strains vs total load appear in Fig. 5a. No loss of rigidity or local buckling resistance was observed. The strains at the cap edges, locations 1 and 2, were unsymmetrical, as shown in Fig. 5b. Strains at location 1 decreased, whereas those at the other edge increased. In other words, the cap bent horizontally in its own plane. Bending strains (curvatures) of this part (see Fig. 5c) resembled the known trends of column buckling with imperfections, leading to the conclusion that the cap actually buckled prior to the overall failure of the stiffener. This phenomenon indicated that, as load was increased, cap buckling was initiated, leading to a premature collapse of the overall section. Cyclic loadings affected neither the initial buckling loads nor the overall behavior. This result differs from that observed in the stiffener panel tests of Ref. 16.

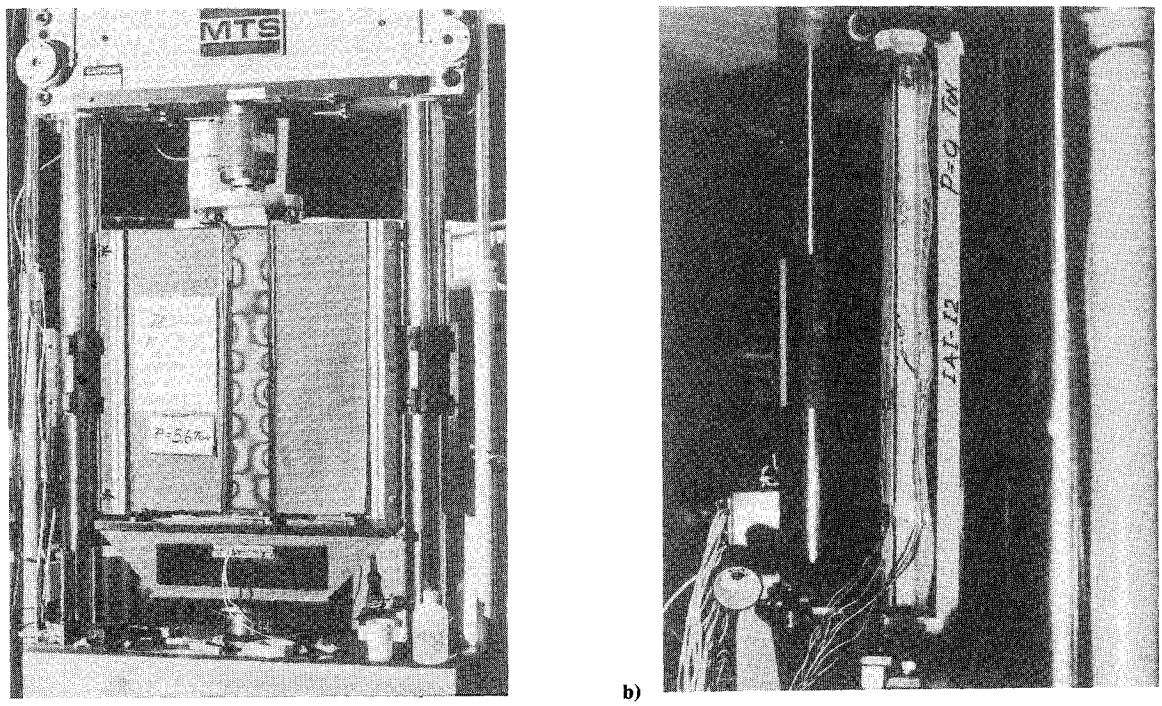

Fig. 3 Specimen I2 and I3 with length = 680 mm: a) buckling-mode shapes; b) skin-edge deflections at P = 9000 kg prior to failure.

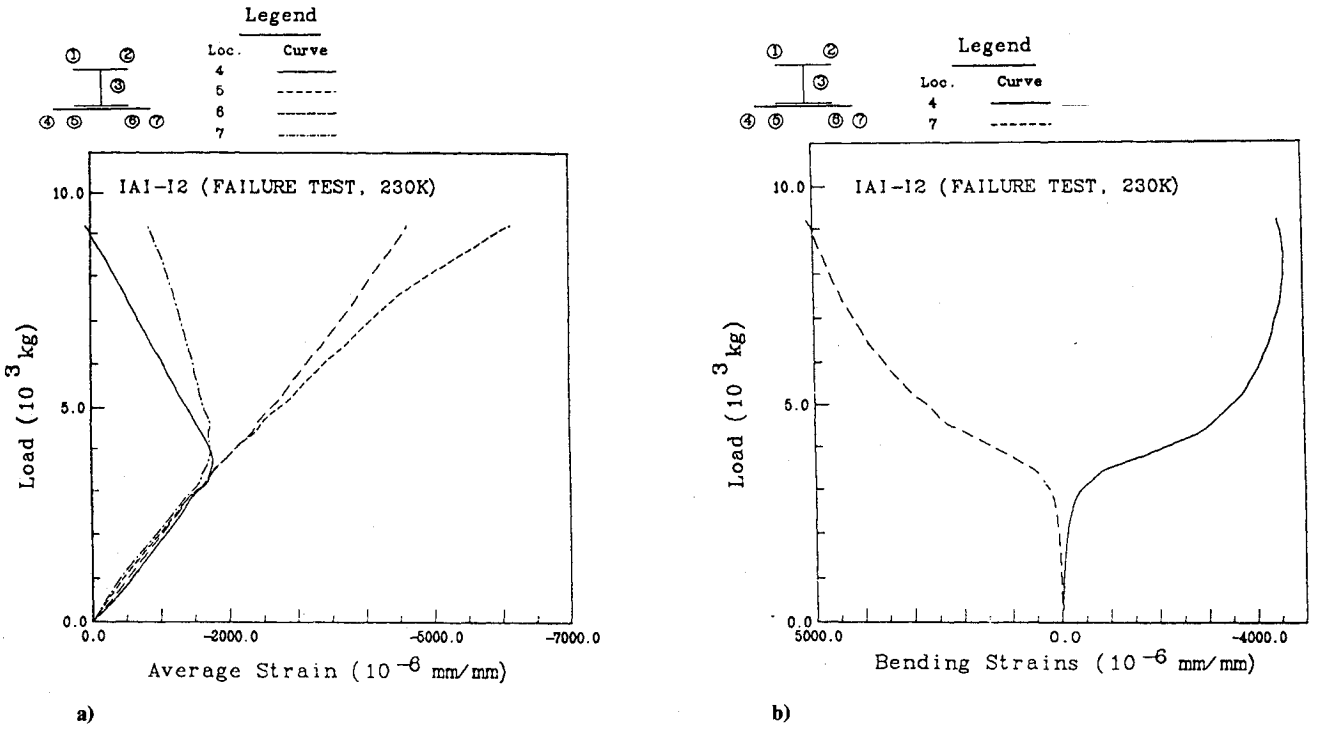

Fig. 4 Load vs longitudinal strains at attached skin edges and flange at midspan, after 230k cycles, length = 680 mm: a) average strains; b) bending strains.

Another question this study attempted to answer was whether an analysis based on an undeformed section (beam analysis) was correct and justified. In general, the use of beam analysis is justified as long as the section shape is preserved. Based on test data, the section shape here was preserved only for loads below the initial buckling level. Hence, an analysis based only on the stiffener section is recommended for loads above the initial buckling level. Strain distribution revealed that above the initial buckling load some eccentricity was induced, either because of changes in the boundary conditions at initial buckling load level or as a result of different imperfections in the two sides of the skin. Cyclic loading effects on the distribution were minor and insignificant.

The I3 behavior was nearly identical to that of I2; collapse, which occurred at 10,200 kg (see Fig. 6a) was lower than predicted but higher than the I2 failure load. This time, failure was initiated by delaminations in the cap and followed by cracks in the skin.

Crippling strength capacity was determined by testing the short specimens to failure. Strains were monitored only at midspan by strain gauges placed at the center of each part of the stiffener. Irregularities at the loaded ends affected be-

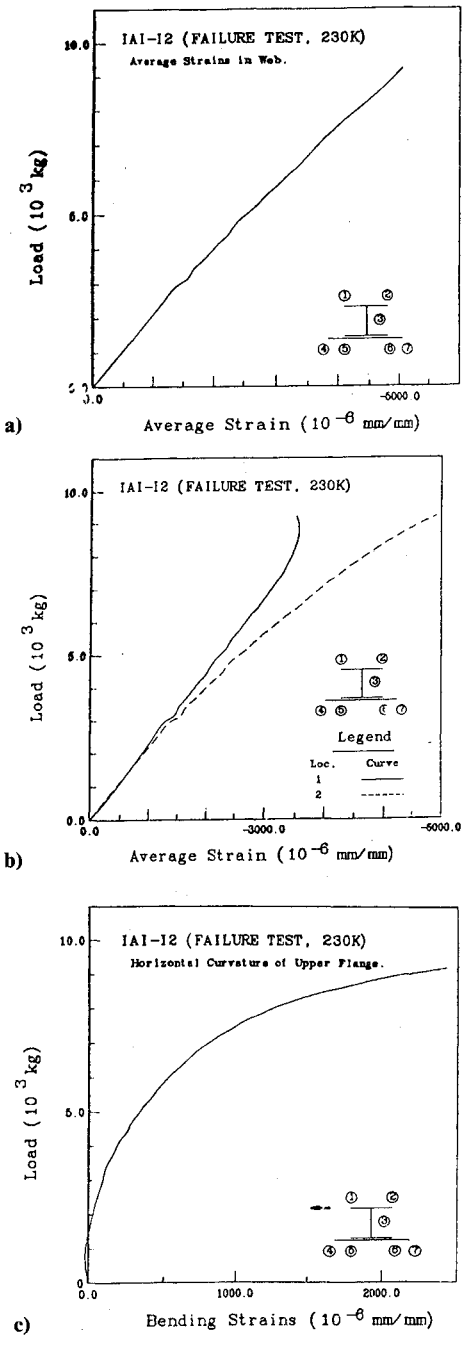

Fig. 5 Longitudinal average strains for specimen I2 at mid-span, after 230k cycles, length = 680 mm: a) center of web; b) cap edges; c) cap horizontal bending.

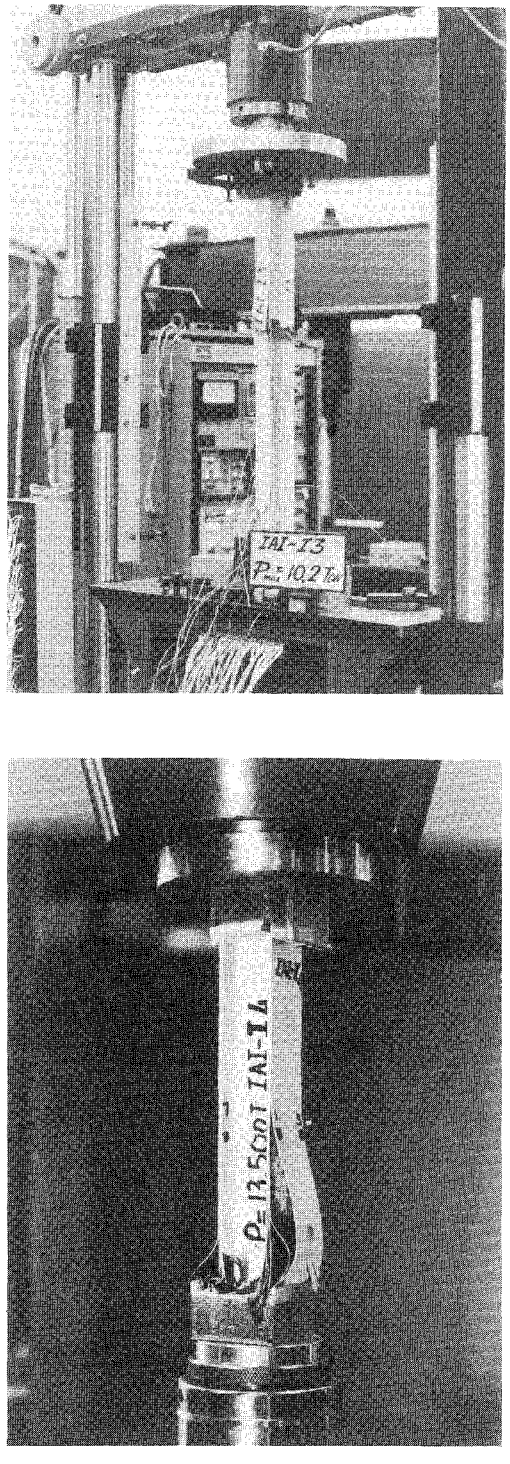

Fig. 6 Failure patterns: a) specimen I3; b) crippling specimen I4.

havior, causing premature collapse and leading to a large scatter in the results (see Table 2). Failure was always associated with cracks at the lower end of the flanges (Fig. 6b).

B. J Stiffener

The first specimen, J1, was used for reference and was monitored by strain gauges similar in pattern to I1. Initial buckling and failure load levels were determined by loading the specimen to failure. Buckling-mode shape formation started at 2200 kg, and the shapes became fully formed at 2600 kg (see Fig. 7a). The buckling mode shapes were different than those of the I stiffener. With J1, only one longitudinal wave was observed. Each edge of the skin was displaced opposite the other, yielding the pattern shown in Fig. 7a. Stiffener deformations, prior to failure, were large, as shown in Fig 7b. Failure, which occurred at 3875 kg, was associated with delaminations

Table 2 Crippling strength of short I and J stiffeners

	Failure[a]		Local buckling	
Specimen	Load, kg	Maximum strain	Load, kg	End short, mm
I4	13,500	9,775	6,300	1.6
I5	9,500	9,075	6,500	1.92
I6	11,750	10,547	7,000	1.92
J4	8,000	8,743	4,000	1.56
J5	7,500	8,202	4,250	1.65

[a]Strains are measured in microstrains, 10^{-6} mm/mm.

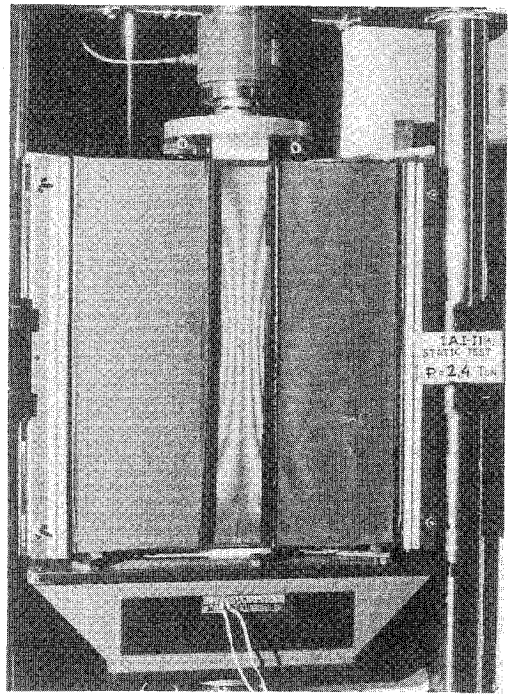

Fig. 7a Buckling-mode shapes.

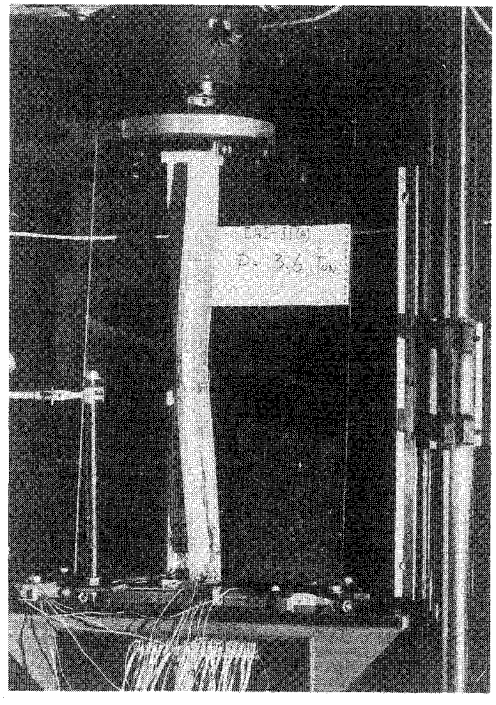

Fig. 7b Stiffener deflections at P = 3600 kg.

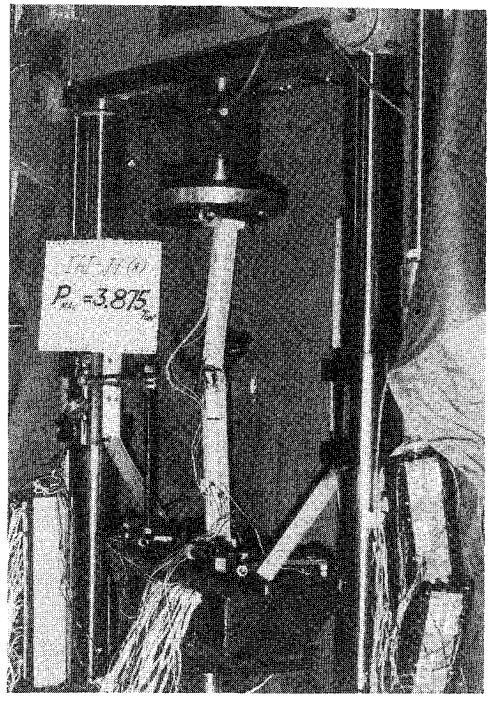

Fig. 7c Failure patterns for J1.

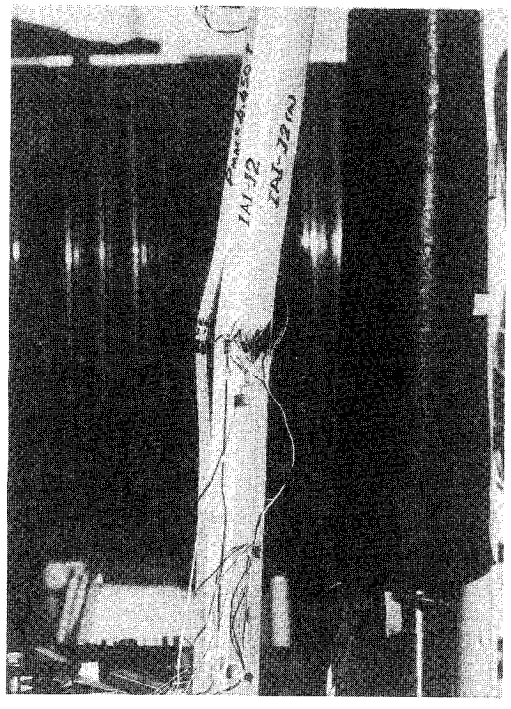

Fig. 7d Failure patterns for J2.

in the cap and cracks and fiber breakage in the skin at midspan (Fig. 7c). No separation of skin from the stiffener was detected although strain level at failure was around 0.9%.

The second specimen, J2, was the same as the first, but the instruments placed in similar fashion to the I2 strain gauge pattern. The specimen was tested under cyclic compression to 250k cycles (see Table 3). The buckling-mode shapes were the same as for J1, but they occurred at a lower load level (Fig. 7a). Residual strength test, which followed the cyclic loading program, yielded a failure load of 4450 kg, which was about 20% higher than the reference collapse load. Failure pattern was nearly identical to that of J1 (Fig. 7d).

The local and overall behaviors are shown in graphical form in Figs. 8 and 9. Average and bending strains of the upper flange and the attached skin, at locations 1–4, are described in Figs. 8. Loss of axial rigidity at locations 1 and 4 was observed at initial buckling load level (Fig. 8a) and was expressed by a reduction in the average compressive strains. The reduction in strains at the skin edges was associated with an increase in the compressive strains at locations 2 and 3. Beam analysis using the gross section is justified for loads below initial buckling level; for loads above this level, only the stiffener section should be considered. The behavior above initial buckling-load level did not follow that of an unsymmetrical section.

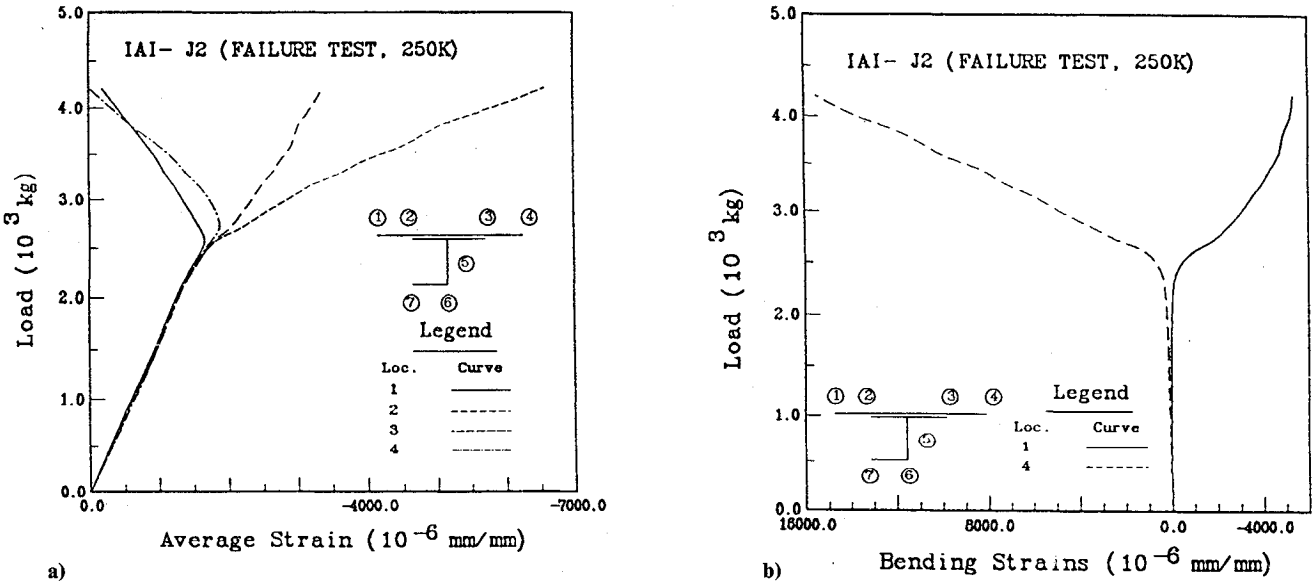

Fig. 8 Longitudinal strains at skin and flange edges at midspan for J2 after 250k cycles: a) average strains; b) bending strains.

The compression-tension strains in the lower flange indicated that the cap buckled prior to the collapse of the stiffener. In view of these results, an analysis that modeled the structure as an assembly of plates interconnected through equilibrium and compatibility conditions was more appropriate.

The unsymmetrical behavior of the stiffener is demonstrated through the bending strains of the skin edges at locations 1 and 4 (Fig. 8b). The displacement at location 4 was larger compared to the other edge, location 1, owing to the nonsymmetrical bending of the section. Local buckling or bending of various parts of the stiffeners appears in Figs. 9. An abrupt change in the behavior was observed at initial buckling load level. Average and bending strains of the web are described in Figs. 9a and 9b, respectively. The web axial rigidity was lost temporarily at 2440 kg and regained at 3000 kg (see Fig. 9a). The abrupt change was due to the initial buckling, which was related to the change in behavior of locations 1 and 4. Web vertical bending strains (curvatures) followed the trends of column buckling as the load was increased toward failure (Fig. 9b). Horizontal bending of the upper flange started at the initial buckling level (Fig. 9c). Cap horizontal bending is described in Fig. 9d. A small increase of load, above 3530 kg, was associated with a decrease in the average compressive strains and an excessive growth in the bending strains, leading to the conclusion that this part experienced buckling.

The cyclic loading program did not affect the local or overall buckling behavior, whereas failure load level was increased by about 20% compared with that of the reference specimen.

Cap construction of the third specimen, J3, was different and consisted of 50% more continuous plies from the web to the cap than did the previous specimens (see Fig. 1c). Some differences in behavior were also observed. Initial buckling (Fig. 10a) was distinct based on location 4 data, but blurred when location 1 was used, probably because of large imperfections. Buckling-mode shapes were nearly identical to those of J2. Web behavior was different (see Fig. 10b), and the loss of axial rigidity reported for the previous specimen did not occur, probably because of local buckling of the web.

Failure occurred at 4800 kg, which was about 30% above the reference failure load and 10% above that of the J2 specimen. Collapse was associated with cap delaminations and cracks in the skin at midspan (Fig. 11a).

Only two J-shaped specimens were tested for crippling strength and these yielded failure loads of 8000 kg (for the J4 specimen) and 7500 kg (for J5); more details appear in Table 2. Failure mode was associated with delaminations in the flanges and cracks in the web (Fig. 11b). Maximum measured average strains around failure were in the range of 0.8–1.1%.

Prediction of the failure of a stiffened composite panel using the results of this study correlated well with test results reported in Ref. 16.

Table 3 Summary of long J stiffeners, strains, buckling, and failure loads

Specimen	Cyclic loading range, kg	Total number of cycles	Initial buckling Load, kg	Initial buckling Strains[a]	Failure load, kg
J1	Static	—	2760	1758(1)	3875
			2290	1758(4)	
J2	1900–2500	250,000	2590	1638(4)	4450
			2750	1732(1)	
J3	1800–2450	250,000	2400	1429(4)	4800
			3000	1743(1)	

[a]Numbers in parentheses are strain gauge locations (see Fig. 8). Strains were measured in microstrains, 10^{-6} mm/mm.

III. Analysis

Buckling behavior of the J stiffener was investigated analytically with an in-house-developed program, PBCOMP.[18,19] The J2 geometrical and mechanical properties were used for data.

The program models any flat, longitudinally stiffened panel made of plate strips and connected transversely through equilibrium and compatibility conditions. The field equations are nonlinear and allow for large displacements with small rotations. The nonlinear equations are expressed in terms of two unknowns, Airy stress function and the lateral displacement. They are solved by resolving the two unknown functions into eigenfunctions in the longitudinal direction and applying a finite difference scheme in the transverse direction. The form of the imperfections consists of the eigenfunction shapes longitudinally and a constant or sine function in the transverse direction. Galerkin procedure is used to minimize error in the truncation process. Then, by means of Newton's method, the nonlinear set of equations is converted into a linear sequence. The use of plate strips allows for local buckling as well as for overall responses.

PBCOMP is capable of dealing with arbitrary boundary conditions, longitudinally as well as transversely. The boundaries can be loaded by combined in-plane loads as well as by a longitudinal, uniform, end-shortening loading pattern.

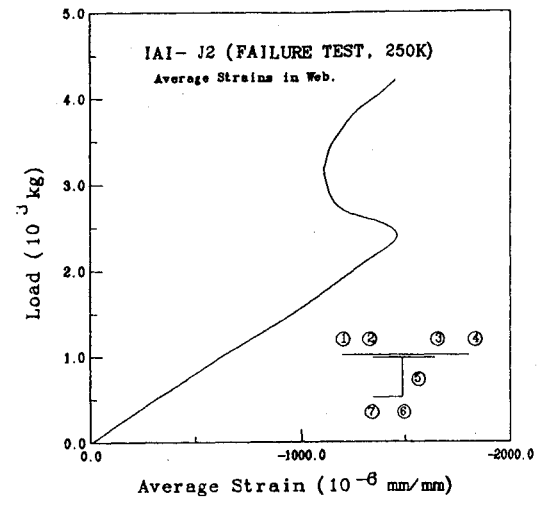

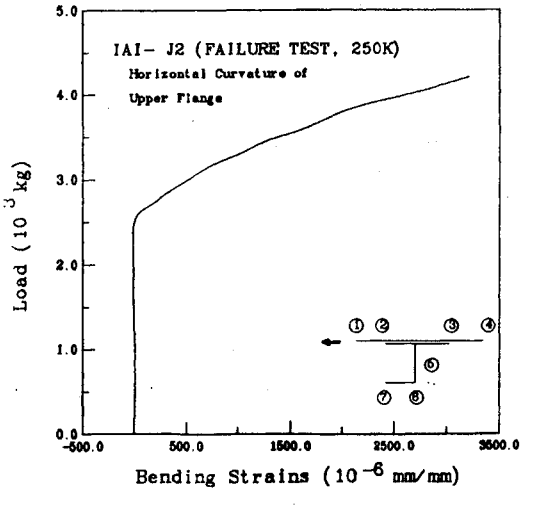

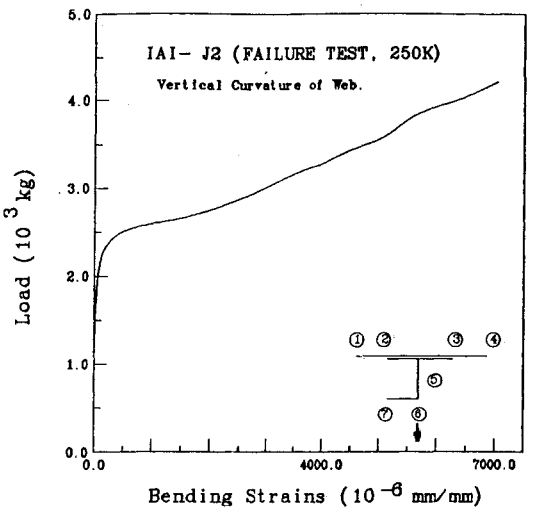

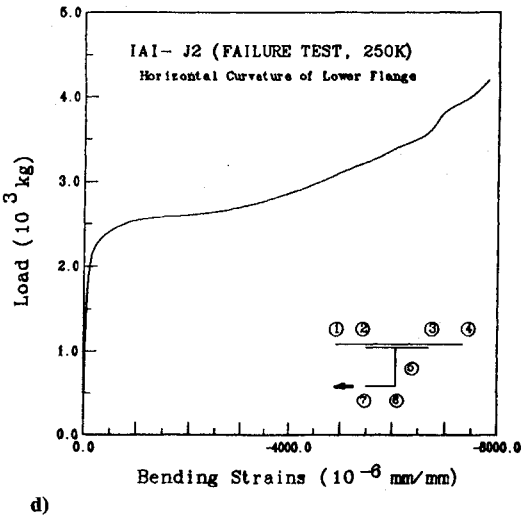

Fig. 9 Specimen J2 at midspan after 250k cycles: a) longitudinal average strains at web center; b) bending strains of web in vertical direction; c) horizontal bending of the upper flange; d) cap horizontal bending.

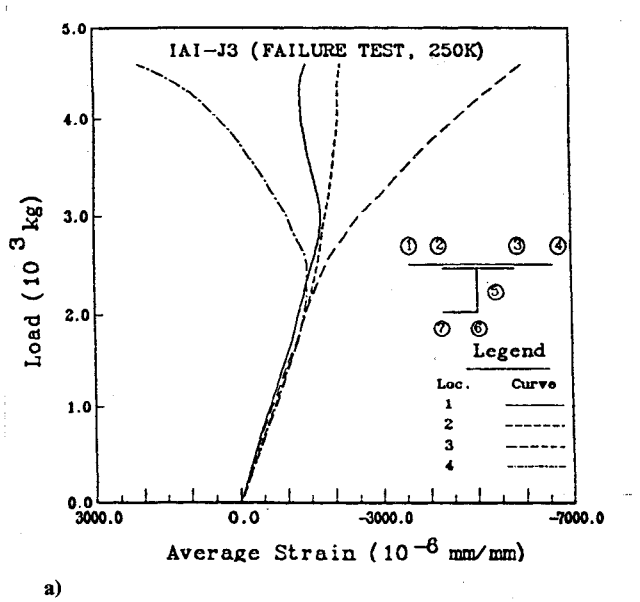

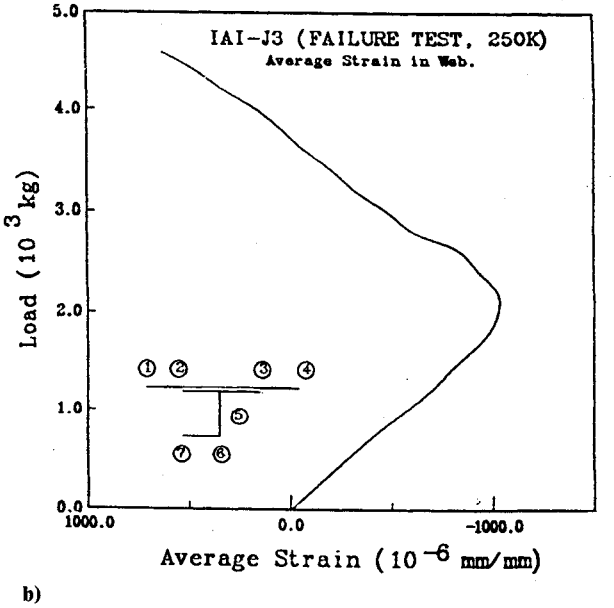

Fig. 10 Longitudinal average strains for specimen J3 at midspan after 250k cycles: a) at attached skin; b) at web center.

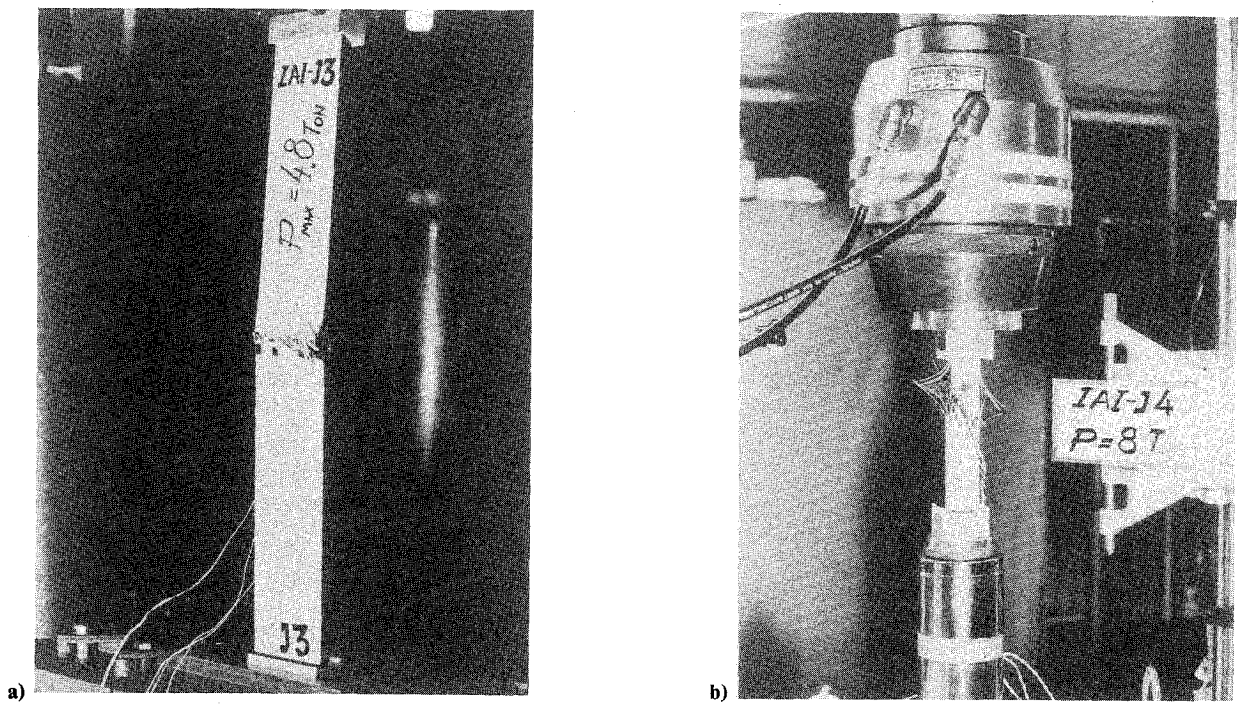

a) b)

Fig. 11 Failure patterns: a) specimen J3 at P = 4800 kg; b) crippling specimen J4.

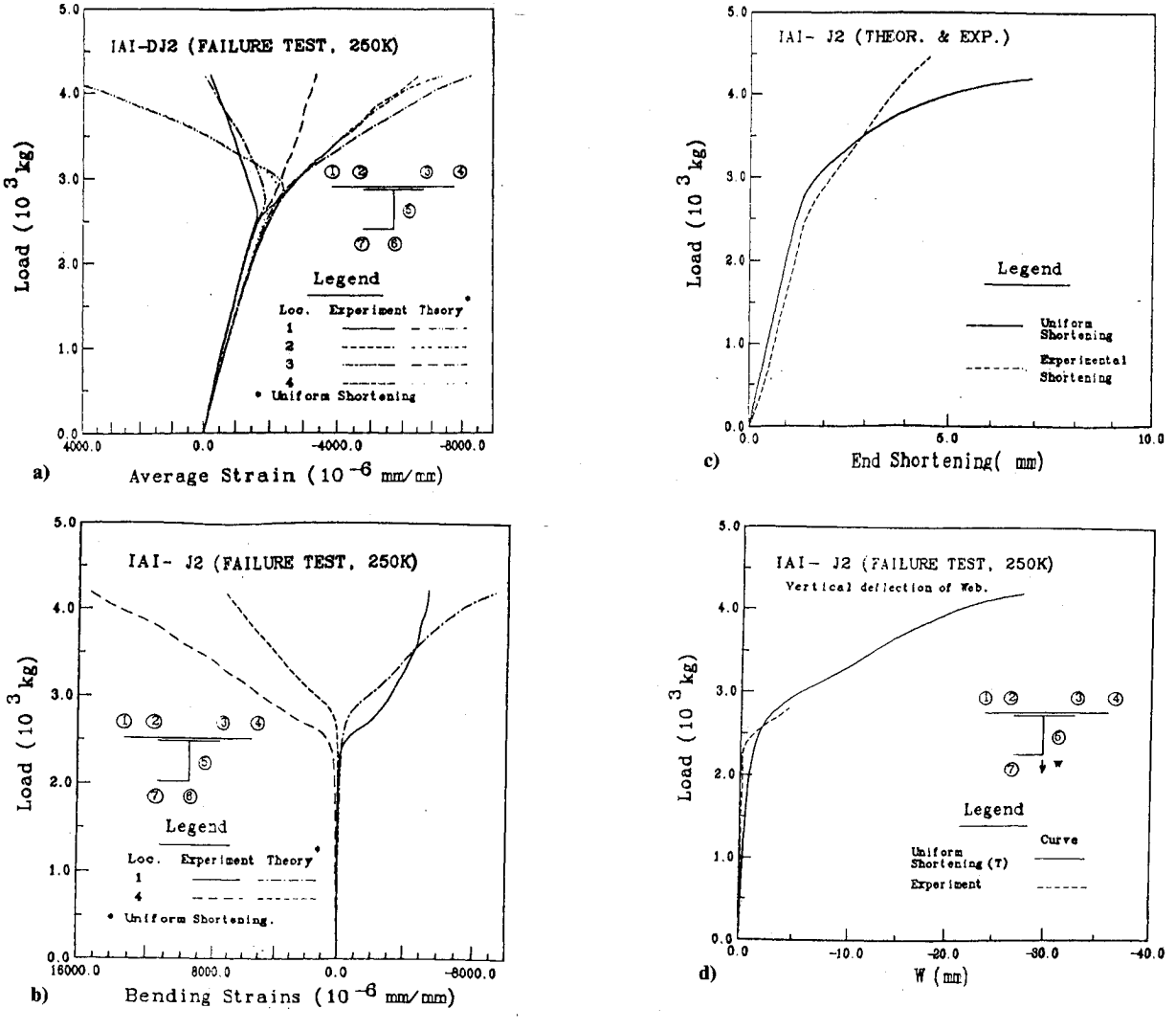

Fig. 12 Analytical and experimental results for specimen J2: a) average strains; b) bending strains; c) end shortening vs applied load; d) out-of-plane deflections of cap-web intersection point.

Laminate layup can be arbitrary and is not limited to any special construction. Stiffener geometry may consist of any thin-walled shape. Output may include internal stress resultants, bending moments, deformations, and end shortening, as well as curvatures (bending strains) and average strains.

The analytical model for specimen J2 assumed that the various plates were clamped at their longitudinal ends, where they were loaded, and were free at their transverse sides. The equivalent, uniform, end-shortening loading distribution was defined by redistributing the total applied load according to the elastic axial rigidity of each plate strip. The distribution was assumed to be uniform within each strip width and unchanged during the loading sequence.

Comparisons of the analytical results with the experimental are shown in Figs. 12. Average and bending strain comparisons for locations 1-4 appear in Figs. 12a and 12b, respectively. The various results correlated well as long as initial buckling-load level was not reached. As load was increased, the analytical results had the same trends but with higher numerical values. The results of end shortening vs applied load, experimentally and analytically, are described in Fig. 12c. Analytical out-of-plane deformations at the web-flange intersection point, described in Fig. 12d, compared well with the experimental deformations. Test results were limited to 2800 kg because of excessive deformations at higher loads.

The discrepancies in the results occurred only in the nonlinear range. The analytical model was loaded by a constant distribution, based on axial rigidities, which remained unchanged during the entire loading sequence. This distribution was correct as long as each plate maintained its axial rigidity. Above initial buckling-load level, the attached skin lost its rigidity, thus yielding a different load distribution; loads previously carried by these parts were transferred to the stiffer regions of the section. This change in loading was associated with smaller deformations since the majority of the load was carried by stiffer regions. In the analytical model, the deformations were larger compared to the experimental results because the load distribution was unchanged during the loading sequence.

IV. Conclusions

A combined experimental and analytical investigation was conducted to study the buckling and postbuckling behavior of selected graphite/epoxy stiffeners loaded in axial compression. I- and J-shaped stiffeners with an attached skin, 90 mm wide, were examined.

The overall behavior was usually associated with initial buckling of the attached skin and beam-column buckling of the stiffener section. The behavior of the various parts of the stiffener was abruptly changed as the load passed through the initial buckling level.

Predictions of failure loads, based on a typical stiffener section that included an attached effective width skin, proved to be satisfactory, regardless of section shape. Cyclic-type loading had favorable effects on the failure loads, whereas only minor changes were observed at initial buckling-load levels. The failure loads of the cycled specimens were always higher than those of the statically loaded reference specimens.

The J stiffener, specimen J3, which had more continuous plies from the web to the cap, had a failure load about 10% higher compared to sections having less continuous plies. Thus, performance improvement can be achieved without weight increase through small changes in design.

Failure pattern always included delaminations in the cap and cracks and fiber breakage in the attached skin. No separation of stiffener from skin was observed although strain level, at flange-skin intersection points, was between 0.8 and 1.0%.

Analytical predictions based on gross section, including the attached skin, were within engineering accuracy, provided that the principal moments of inertia were used. In this method, the coupling effects of local buckling on the overall behavior were neglected. Section shape was not preserved as load approached failure level; thus, an analysis using PBCOMP, which allows distortion of the cross section, is recommended.

Two typical stiffener shapes were examined, I and J, because these are often used in the design of stiffened panels. The I-shaped stiffener weighed 20% more than the J type and its carrying-load capacity was 100% higher. The overall behavior of the I-shape stiffener was associated with smaller deformations, and it proved to be stiffer compared to the J-shaped stiffener.

Analytical results based on PBCOMP, and using the tested specimen for data, were in good agreement with the experimental findings. An improvement in the analytical predictions can be achieved if the load distribution is allowed to change during the loading sequence on the basis of uniform end-shortening conditions.

References

[1]Wagner, H., "Ebene Blechwandtrager mit Sehr Dunnem Stegblech," Flugtechnik und Motorluftschiffahrt, Bd. 20, 1929.

[2]Koiter, W. T., "On the Stability of Elastic Equilibrium," Air Force Flight Dynamics Lab., Wright-Patterson AFB, OH, AFFDL-TR-70-25, 1976.

[3]Ashton, J. E., and Waddoups, M. E., "Analysis of Anisotropic Plates," *Journal of Composite Materials,* Vol. 3, Jan. 1969, pp. 148-165.

[4]Ashton, J. E., and Waddoups, M. E., "Analysis of Anisotropic Plates II," *Journal of Composite Materials,* Vol. 3, July 1969, pp. 470-479.

[5]Ashton, J. E., "Anisotropic Plate Analysis-Boundary Conditions," *Journal of Composite Materials,* Vol. 4, April 1970, pp. 163-167.

[6]Ashton, J. E., and Love, T. S., "Experimental Study of the Stability of Composite Plates," *Journal of Composite Materials,* Vol. 3, April 1969, pp. 230-242.

[7]Agarwal, B. L., "Post-Buckling Behavior of Composite Shear Webs," *AIAA Journal,* Vol. 19, No. 7, 1981, pp. 933-939.

[8]Kudva, N. J., and Agarwal, B. L., "Post-Buckling Analysis of Stiffened Composite Shear Panels—Theoretical Analysis and Comparisons with Experiments," *Proceedings of the 102nd ASME Winter Annual Meeting,* Nov. 1981, pp. 221-229.

[9]Starnes, J. H., Jr., and Rouse, M., "Post-Buckling and Failure Characteristics of Selected Flat Rectangular Graphite-Epoxy Plates Loaded in Compression," AIAA Paper 81-0543, April 1981.

[10]Starnes, J. H., Jr., and Rouse, M., "Post-Buckling Behavior of Selected Flat Stiffened Graphite-Epoxy Panels Loaded in Compression," *AIAA Journal,* Vol. 23, No. 8, 1985, pp. 1236-1246.

[11]Chia, C. Y., *Nonlinear Analysis of Plates,* McGraw-Hill, New York, 1980.

[12]Leissa, A. W., "Analysis of Laminated Composite Plates and Shell Panels," Air Force Wright-Patterson Aeronautical Lab., Wright-Patterson AFB, OH, AFWAL-TR-85-3069, Jan. 1985.

[13]Dickson, J. N., Cole, R. T., and Wang, J. T. S., "Design of Stiffened Composite Panel in the Post-Buckling Range," *Fibrous Composite in Structural Design,* edited by E. M. Leone, D. W. Oplinger, and J. J. Burke, Plenum Press, New York, 1980, pp. 313-327.

[14]Brooks, W. G., "The Design and Construction of a Post-Buckling Carbon Fibre Wing Box Structure," International Congress of Aeronautical Sciences, Paper 86-4.2.1, 1986.

[15]Weller, T., Kollet, M., Libaii, A., and Singer, J., "Durability Under Repeated Buckling of Stiffened Shear Panels," *Proceedings of the 14th ICAS Conference,* Toulouse, France, Sept. 1984, pp. 932-942.

[16]Segal, A., Siton, G., and Weller, T., "Durability of Graphite-Epoxy Stiffened Panels Under Cyclic Post-Buckling Compression Loading," *Proceedings of the ICCM VI/ECCM,* London, July 1987.

[17]Renieri, M. P., and Garrett, R. A., "Investigation of the Local Buckling, Postbuckling and Crippling Behavior of Graphite/Epoxy Short Thin-Walled Compression Members," McDonnell Aircraft Co., MDC-A7091, July 1981.

[18]Sheinman, I., and Frostig, Y., "Post-Buckling Analysis of Stiffened Laminated Panels," *Journal of Applied Mechanics,* Vol. 55, No. 3, 1988, pp. 635-640.

[19]Sheinman, I., Frostig, Y., and Segal, A., "Bifurcation Buckling Analysis of Stiffened Composite Laminated Panels," *Buckling of Structures—Theory and Experiments,* Vol. 19, Josef Singer Anniversary Volume, Studies in Applied Mechanics, edited by Elishakoff et al., Elsevier, Amsterdam, 1988, pp. 355-380.